J. Am. Soc. Mass Spectrom. (2014) 25:351–367
DOI: 10.1007/s13361-013-0783-x

RESEARCH ARTICLE

# Photofragmentation of Halogenated Pyrimidine Molecules in the VUV Range

Mattea Carmen Castrovilli,[1,2] Paola Bolognesi,[1] Antonella Cartoni,[3] Daniele Catone,[4] Patrick O'Keeffe,[1] Anna Rita Casavola,[1] Stefano Turchini,[4] Nicola Zema,[4] Lorenzo Avaldi[1]

[1]CNR-IMIP, Area della Ricerca di Roma 1, Monterotondo Scalo, Italy
[2]Dipartimento di Chimica G. Ciamician, Università di Bologna, Bologna, Italy
[3]Dipartimento di Chimica e Tecnologie del Farmaco, Università degli Studi di Roma Sapienza, Rome, Italy
[4]CNR-ISM, Area della Ricerca di Roma 2, Roma, Italy

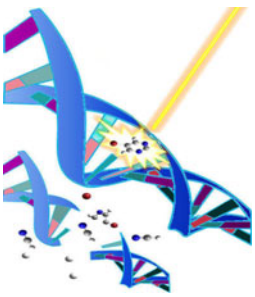

**Abstract.** In the present work, we studied the photoinduced ion chemistry of the halogenated pyrimidines, a class of prototype radiosensitizing molecules, in the energy region 9–15 eV. The work was stimulated by previous studies on inner shell site-selective fragmentation of the pyrimidine molecule, which have shown that the fragmentation is governed by the population/formation of specific ionic states with a hole in valence orbitals, which in turn correlate to accessible dissociation limits. The combined experimental and theoretical study of the appearance energies of the main fragments provides information on the geometric structure of the products and on the role played by the specific halogen atom and the site of halogenation in the dissociation process. This information can be used to gain new insights on the elementary mechanisms that could possibly explain the enhanced radiation damage to the DNA bases or to the medium in which the bases are embedded, thereby contributing to their radiosensitizing effect.

**Key words:** Photofragmentation, Halogenated pyrimidines, Appearance energy, G3B3, VUV synchrotron radiation, Radiation damage, Mass spectrometry

Received: 6 June 2013/Revised: 11 November 2013/Accepted: 17 November 2013/Published online: 3 January 2014

## Introduction

The attempts to understand the effects of ionizing radiation in biological systems from the microscopic physical chemistry point of view is an example of the increasing efforts in multidisciplinary research, bridging the gap between physics, chemistry, and biology. The harmful influence of electromagnetic radiation and high energy particles on biological systems has long been known, but the microscopic mechanisms, acting at the single molecule level, are just recently being unravelled [1]. This has led to significant, and sometimes unexpected, 'discoveries' in the understanding of the general picture of radiation damage [2]. Selective irradiation of the nucleus or the cytoplasm shows the DNA to be the most sensitive target in the cell [3]; its damage leads to dramatic consequences such as cell death or mutagenesis. From the physical chemistry point of view, the DNA damage can be tracked down to processes occurring on the femto- to nano-second timescale and involving different parts of the DNA, from nucleotides down to their building blocks, the purinic and pyrimidinic bases [4, 5 and references therein]. Single/double strand breaks of the DNA resulting from radiation damage can be studied and quantified by well-known techniques, such as electrophoresis, while insights into the microscopic processes can be obtained by spectroscopic techniques including (e.g., photoelectron and photo ion spectroscopies [1]). The latter techniques have the invaluable property that they are able to disentangle the effects induced directly on the isolated molecule itself from the indirect effects induced by the surrounding environment.

The understanding of the processes occurring between the energy absorption and the manifestation of the damage may allow the control and a proper handling of the process itself.

**Electronic supplementary material** The online version of this article (doi:10.1007/s13361-013-0783-x) contains supplementary material, which is available to authorized users.

*Correspondence to:* Mattea Castrovilli; *e-mail:* matteac@gmail.com

A typical example is represented by the radiosensitizers used in radiotherapy. These are specific agents suitably chosen to increase selectively the radiosensitivity of tumor cells while limiting the effects on the surrounding normal tissue. Among them, an important class is represented by the halogenated pyrimidines, which are compounds structurally similar to the cytosine, thymine, and uracil DNA/RNA bases, where a member of the halogen group of elements (fluorine, chlorine, bromine, and iodine) is bound to the pyrimidinic ring. Due to resemblance to the cytosine, thymine, and uracil structure, these halogenated compounds may be selectively incorporated into the DNA of fast reproducing tumor cells. When sufficient quantities of the altered DNA molecules are present, the harmful effects of radiation are increased.

Different mechanisms have been proposed to explain the radiosensitizing effect induced by the selective incorporation of halogenated pyrimidine bases into the DNA of tumor cells. These span from the formation of transient negative ion resonances followed by dissociative electron attachment (DEA) [2], due to the scattering of low kinetic energy secondary electrons produced by the ionization of the surrounding medium, to the direct absorption of X-ray radiation. Although a large body of results has been produced in the study of the DEA process in DNA/RNA bases [6] and their halogenated analogues [7–9], far less effort has been devoted to the investigation of the 'direct' effects attributable to the absorption of VUV, soft-, and hard X-ray radiation by the DNA constituents. Nevertheless, in the case of halogenated analogues of DNA bases, the formation and electron decay of core vacancies has long been pointed out as a leading channel in the selective tumor damage induced by these radiosensitizers [10, 11]. A selective and enhanced molecular fragmentation of the halogenated species has also been proposed and investigated [1]. Fluoro- (FdU) and bromo-deoxyuridine (BrdU) and gemcitabine, a fluorine substitute of deoxycytidine, are just some of the most common analogues of pyrimidines used in radiotherapy. A broad investigation of their building block, the pyrimidine, and halogenated pyrimidine molecules, is expected to provide useful insight into relevant mechanisms which, acting at the single molecule level, might explain their radiosensitizing effects.

From an experimental point of view, the pyrimidine molecule presents the following advantages: (1) it has the fundamental structure of the cytosine, thymine, and uracil DNA/RNA bases and it shares with the bases many of its properties and (2) it can be easily produced in the gas phase because of its relatively high vapor pressure at room temperature that does not require heating of the sample, thus removing the risk of thermal decomposition. Previous fragmentation [1, 12–15] and ionization studies of pyrimidine and halogenated pyrimidines in the valence [16–18] and inner shell regions [19–22] have provided a comprehensive spectroscopic characterization of these molecules. In the pyrimidine case, taking advantage of the non-equivalent binding energies of the localized C and N core electrons, time-of-flight mass spectrometric measurements have been performed at several photon energies across the excitation/ionization thresholds of the C and N K-edges using tunable synchrotron radiation in the soft X-ray range. These experiments clearly revealed both the photon energy dependence and the site-selectivity of the molecular fragmentation of pyrimidine. The more selective resonant Auger electron-ion coincidence measurements [1], which focus on the one-electron decay to the lowest electronic states of the pyrimidine cation, proved that the fragmentation pattern is determined by the final, rather than the intermediate, site-selected, state. The so-called 'molecular knife' effect [23–25], where a localized core excitation is proposed to control selective molecular bond breaking was found to be, in the pyrimidine case, an indirect effect. The fast de-excitation of the intermediate states via spectator/participator resonant Auger decay affects the branching ratio of the populated valence electronic states with respect to direct ionization. Together with the selective fragmentation of these same valence shell electronic states already observed by Plekan et al. [26], the resonant Auger electron-ion experiments in pyrimidine showed the crucial role played by the valence shell in the fragmentation dynamics also when soft X-rays are absorbed. In the investigated ionization energy range 9–15 eV of the photoelectron-ion [26] and resonant Auger electron-ion coincidence experiments [1], the dominant fragmentation patterns of the energy selected electronic states appear to correlate to the nearest appearance potential.

Stimulated by these results in pyrimidine, we have undertaken a joint experimental and computational study of the photofragmentation of the 2Br-, 2Cl-, and 5Br- pyrimidine molecules in the VUV range. Although halogen-substituted pyrimidines have a similar structure as the pyrimidine molecule and share many of its photophysical and photochemical properties, their photodissociation dynamics may be quite different. These targets have been chosen with the purpose of investigating the effect of the specific halogen atom and the site of halogenation on the fragmentation dynamics.

## Experimental and Methods

The experiments were performed at the 'Circular Polarization' (CiPo) beamline 4.2 [27] of the Elettra synchrotron radiation source, Trieste, Italy. In the present VUV fragmentation measurements, the radiation of the electromagnetic elliptical undulator was monochromatized by an aluminium normal incidence monochromator (NIM) that covers the photon energy range 5–17 eV (resolving power of about 1000). The setup consists of five electrostatic lenses that focus and accelerate the ions from the region of interaction to the quadrupole mass spectrometer (QMS). This is a commercial QMS (10-4000 u, Extrel (Pittsburgh, PA, USA) 150-QC 0.88 MHz) with a mass resolution $\Delta M/M$ of about 500. It is mounted perpendicular to the photon beam and to the gas source, which is an effusive beam

located at 5 cm from the entrance of the QMS and about 2 mm below the photon beam. The typical flight time of the charged systems is in the order of 5 to 100 μs, depending on the fragment. An overview of the experimental setup is reported in Figure 1.

The pyrimidine molecule is liquid and its halosubstituted compounds are powders at standard ambient temperature (298 K) and pressure (with vapor pressures varying between 0.04 and 22 mbar [28]). In the present setup, the powder of the target under investigation was maintained in a test tube outside the vacuum chamber and admitted into the interaction region through a gas line producing an effusive beam, with a residual gas pressure in the experimental chamber in the order of few $10^{-6}$ mbar (base pressure $5\times10^{-7}$ mbar), sufficient to perform the experiments.

For each target molecule, the experiments consist of the acquisition of the mass spectra at fixed photon energy and the measurement of the photoionization efficiency curves (PECs) of the selected ions.

The mass spectrum of each target was measured at 14 eV, providing an overview of the most relevant fragments at this photon energy (Figure 2). The data reported in Figure 2 were not corrected for the transmission of the QMS, preventing a reliable measure of the absolute branching ratio of the different fragments. However, according to the nominal transmission of the instrument and by comparing the mass spectrum of the pyrimidine molecule measured at 17 eV (Figure 2a) with the spectra reported in the literature [13, 14], we inferred that the transmission of the spectrometer should not introduce major distortions in the range of masses above 40 u. In the second part of the experiment, we obtained the experimental appearance energy (AE) values by measuring the PECs of the parent ion and of the selected fragments as a function of the photon energy (9–15 eV) with an energy step of 20 meV and an acquisition time of about 3 to 10 s/point, depending on the intensity of the measured mass peak. The PECs were normalized to the photon intensity, which was measured simultaneously by a photodiode located at the end of the beamline. The photon energy was calibrated against the auto-ionization features observed in the Ar total photoionization efficiency spectra between the 3p spin orbit components. In the photon energy scans up to 11.7 eV, a lithium fluoride filter was used to remove the second order radiation. Above this energy, the contribution of the second order radiation was evaluated by comparing the $Ar^+$ ion yield measured as a function of the photon energy to its ionization cross-section [29]. This second order contribution was taken into account in the extraction of the PECs.

All the PECs are shown on a linear scale. However, the experimental AE values are determined from their semilog plots by fitting straight lines to the background and to the ion signal in the threshold region (see, for example, the inset of Figure 3a). The photon energy at the intersection of these two lines is the measured AE value at 298 K [$AE_T(exp)$], which is the temperature of the experiment [30]. The uncertainty is estimated to be on the order of 0.05–0.10 eV and depends on the sharpness of the photoionization efficiency curve. Even though the use of the semilog rather than the linear scale has the advantage of increasing the sensitivity of the data analysis procedure [31], it is important to remember that the measured values of AE also depend on the

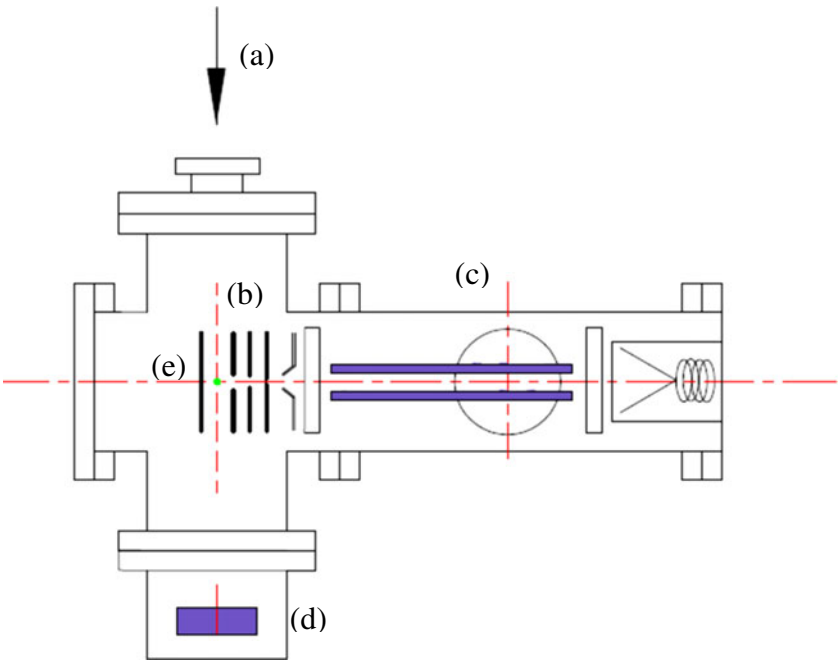


**Figure 1.** Schematic of the experimental apparatus: **(a)** direction of propagation of the photon beam, **(b)** electrostatic lens, **(c)** quadrupole mass spectrometer (QMS), **(d)** photodiode. The effusive gas beam is perpendicular to the plane of the drawing and crosses the synchrotron beam at the interaction region **(e)**

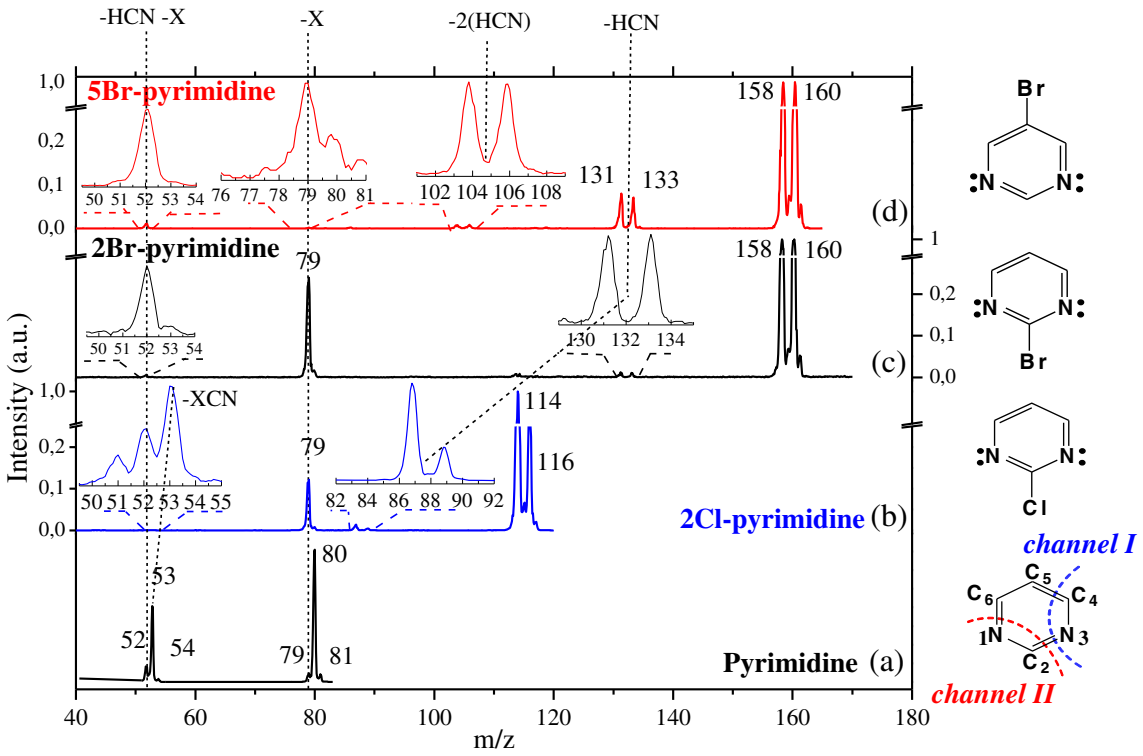


**Figure 2.** The photoionization mass spectra of **(a)** pyrimidine measured at 17 eV photon energy, **(b)** 2Cl-pyrimidine, **(c)** 2Br-pyrimidine, and **(d)** 5Br-pyrimidine recorded at 14 eV photon energy. The break in the y-axis is meant to emphasise low intensity features

sensitivity of the experimental setup (time of acquisition, number of counts, statistics, and efficiency), so that the measured AE have to be considered as the upper limits of the effective AE.

## Thermochemical and Computational Analysis

The AE is the minimum energy required to produce a particular fragment ion. Theoretically, the AE is defined as the difference between the energy of the ground state of the fragments and that of the neutral molecule (i.e., the adiabatic energy of the fragmentation process). In this work, we performed ab initio calculations of the parent ion and some ionic fragments of 2Cl-, 2Br-, and 5Br-pyrimidine using theoretical methods embedded in the Gaussian 09 package of programs [32]. In the photoionization and subsequent fragmentation of a molecule $M$ by monochromatic radiation of energy $hv$, the ionic fragment $m_1^+$, and several neutral fragments $m_i$ are produced

$$M + hv \rightarrow M^+ + e^- \rightarrow m_1^+ + \sum m_i + e^- \quad (1)$$

Let us consider the general process (1) for which the potential barrier to the reverse reaction is assumed to be zero. As already shown by Treager and McLoughlin [30], in the reaction (unimolecular decomposition), the initial translational momentum of the center of mass (CM) and the angular momentum about the CM of the precursor molecule plus the photon is conserved during the reaction. In addition, the total energy of the photon and the precursor molecule must be conserved. If the unimolecular decomposition is sufficiently rapid, the observed appearance energy [$AE_T(exp)$] corresponds to the adiabatic appearance energy [$AE_T(ad)$], which represents the minimum energy to form $m_1^+ + \Sigma m_i + e^-$ from $M$ at temperature $T$.

Chupka [33] has shown that if an extrapolation of a linear post-threshold region can be used to determine $AE_T(exp)$, then

$$AE_0(exp) = AE_T(exp) + E_i \quad (2)$$

where $E_i$ is the internal thermal energy of $M$ effective in dissociation. In such a case, all the rotational and vibrational energy associated with the precursor molecule is effective in dissociation. On this basis and assuming the stationary electron convention for cationic heats of formation [i.e., $\Delta H_T^\circ(e^-)=0$], the $AE$ at 0 K is defined as:

$$AE_0 = \sum [\Delta_f H_0^\circ(m_i)] + \Delta_f H_0^\circ(m_1^+) - \Delta_f H_0^\circ(M) \quad (3)$$

where $\Delta_f H^\circ_0$ is the enthalpy of formation at 0 K. We can derive the AE at 298 K by adding thermal energy correction elements:

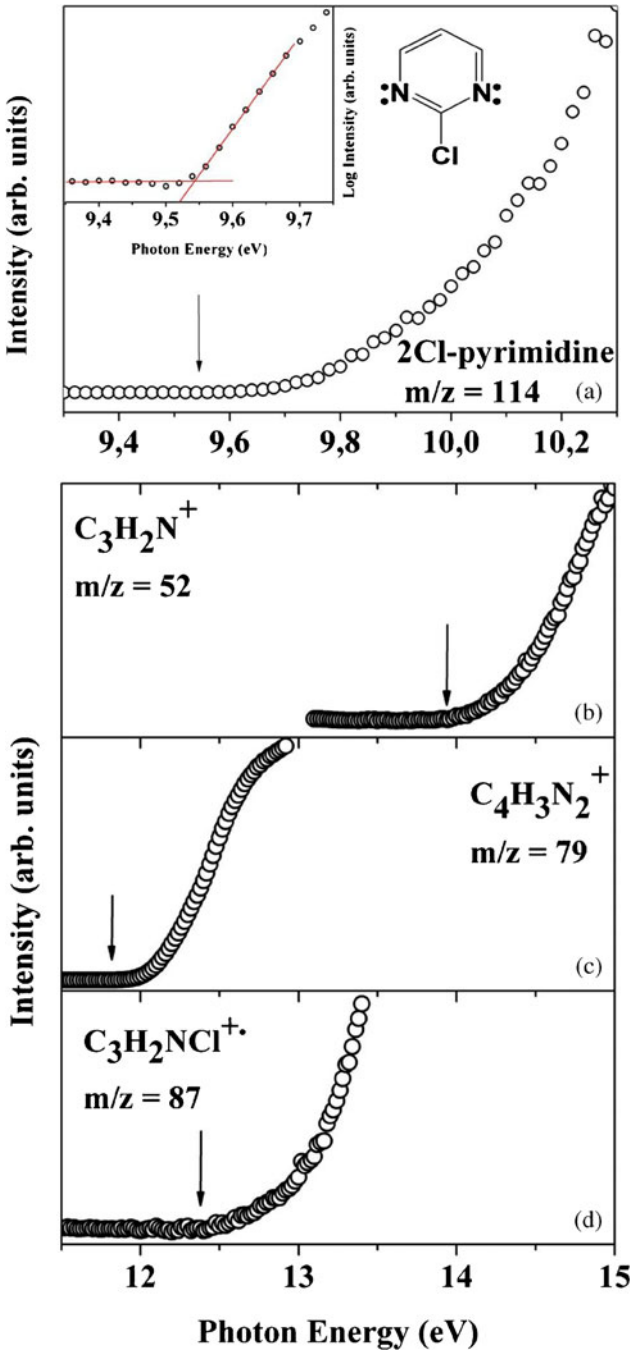


**Figure 3.** Photoionization efficiency curve of the parent ion **(a)** and three of the 2Cl-pyrimidine fragment ions **(b)**, **(c)**, and **(d)**. In the parent ion case, [inset of **(a)**] the threshold region is expanded and reported in log scale. The measured AE values are indicated by an arrow and reported in Table 1

$$AE_{298} = AE_0 - \left\{H^\circ_{298} - H^\circ_0\right\}(M) + {}^5/_2 RT \quad (4)$$

where the term $\{H^\circ_{298} - H^\circ_0\}(M)$ gives the heat of formation of the precursor molecule and *5/2RT* is its translational contribution ($\int_0^{298} C_{Ptrans}(M)dT$), where $C_P$ is the heat capacity at constant pressure.

In the case of the parent ions and direct ionization process, care must be taken with the manipulation of thermodynamic quantities. As noted by Lias and Ausloos [34] for a given molecule, M

$$IE(ad) = \Delta H^\circ_{f0}(M^+) - \Delta H^\circ_{f0}(M) \quad (5)$$

the adiabatic ionization energy, IE(ad), corresponds to the energy difference between the ground vibrational and rotational level of the lowest electronic state of the ion and the ground vibrational and rotational level of the lowest electronic state of the molecule. This is rigorously equal to the difference in the heats of formation of the ion and of the molecule at 0 K. The adiabatic ionization energy is equal to the enthalpy of ionization, which is the difference between the heats of formation of the ion and the corresponding molecule at some temperature above 0 K (298 K in this study), only when the integrated heat capacities of the ion and neutral species are identical ($\int_0^T C_p(M^+)dT = \int_0^T C_p(M)$dT):

$$\Delta H^\circ_T(ionization) = IE(ad) + \left\{H^\circ_{298} - H^\circ_0\right\}(M^+) - \left\{H^\circ_{298} - H^\circ_0\right\}(M) \quad (6)$$

where $\{H^\circ_{298} - H^\circ_0\}(M^+)$ is $\int_0^T C_p(M^+)dT$ and $\{H^\circ_{298} - H^\circ_0\}(M)$ is $\int_0^T C_p(M^+)dT$.

In our case, the differences between the heat capacity of the molecules and the corresponding ions are of the order of 0.008 eV, so the adiabatic ionization potential is expected to be the same as the 298 K enthalpy of ionization within the experimental error.

The relative energies and heat capacity for the reactants and products were calculated using the G3B3 [35] method. To calculate the G3B3 energy, we performed calculations of single-point energies at the levels of MP4/6-31G(*d*), QCSID(T)/6-31G(*d*), MP4/6-31+G(*d*), MP4/6-31G(2*df*, *p*), and MP2(full)/G3 large; G3 large is a modification of the MP2/6-311+G(*3df*,*2p*) basis set. For the fragment ions, we calculated the theoretical AEs at 298 K (Equation 4) using the G3B3 level of the theory. The adopted procedure involves (1) the optimization of the geometry of the fragments at DFT, B3LYP/6-311++G(2d,2p) level, and (2) the calculation of the enthalpy of formation ($\Delta_f H_0$) and the thermal energy correction elements at the G3B3 level. The mean absolute deviation between the G3B3 computed- and literature standard state enthalpies of formation for a selected set of organic molecules is about 0.027 eV [36].

As will be discussed below, some of the final geometries of the studied fragments, even though representing the lowest (i.e., adiabatic), energy config-

uration would involve significant rearrangement of the molecular structure with respect to the neutral molecule. Such rearrangements consist of bond breakings and atom migrations, which can only be obtained by overcoming energy barriers in the potential energy surfaces. The last contribution is clearly not included in the adiabatic calculation, but has to be estimated separately. For this reason, the experimental determination of the AE of a fragmentation pattern can only be higher or equal to the corresponding adiabatic, theoretical value. To investigate such mechanisms, in some cases, we performed a synchronous transit-guided quasi-newton (STQN) method, at B3LYP/6-31G(*d*) level of theory [37, 38], in order to obtain the transition state between selected initial and final configurations. The energy barrier is then calculated at the B3LYP level of theory, as energy difference between the initial and intermediate states. The results of the energetic calculation G3B3 and the optimized geometries are summarized for all the fragments in Figure 6 in the supporting material (SM).

## Results and Discussion

The pyrimidine molecule has a six-membered ring structure, with two N and four C atoms. Its mass spectrum measured at 17 eV photon energy is shown in Figure 2a. We measured the AE of the parent ion (*m/z* 80) and fragment at *m/z* = 52 attributable to the loss of the HCN group (data not shown). The values found (9.23 ± 0.03 and 13.48 ± 0.06 eV, respectively) are consistent with the previous results by Schwell et al. [13] (9.21 ± 0.05 and 13.75 ± 0.10). In the present work, we have investigated the valence dissociation pathways of Br- and Cl- pyrimidine molecules, where the halogen atom is in positions 2 or 5 of the ring, with the purpose of studying the effect of the different halogen substitutions (Cl or Br in the 2Cl- and 2Br-pyrimidine, respectively) and site of halogenation (2 or 5 for the 2Br- and 5Br-pyrimidine, respectively) in the fragmentation dynamics of the pyrimidinic ring. Figure 2b–d shows the mass spectra of the three studied molecules measured at 14 eV photon energy, which is discussed in a section below.

Several fragments/fragmentation channels common to all species are clearly observed in the spectra. They are produced according to the following photoreactions:

$$C_4H_3N_2X + h\nu \rightarrow \mathbf{C_4H_3N_2X^{+\bullet}} + e^- \quad (7)$$

$$C_4H_3N_2X + h\nu \rightarrow \mathbf{C_3H_2NX^{+\bullet}} + HCN + e^- \quad (8)$$

$$C_4H_3N_2X + h\nu \rightarrow \mathbf{C_2HX^{\bullet +}} + HCN + HCN + e^- \quad (9)$$

$$C_4H_3N_2X + h\nu \rightarrow \mathbf{C_3H_2N^{+}} + HCN + X^{\bullet} + e^- \quad (10)$$

$$C_4H_3N_2X + h\nu \rightarrow \mathbf{C_4H_3N_2}^{+} + X^{\bullet} + e^- \quad (11)$$

$$C_4H_3N_2X + h\nu \rightarrow \mathbf{C_3H_3N^{+\bullet}} + XCN + e^- \quad (12)$$

$$C_4H_3N_2X + h\nu \rightarrow \mathbf{C_3H_2N^{+}} + XCN + H^{\bullet} + e^- \quad (13)$$

which can be identified as the formation of the unfragmented parent ion, (Equation 7), and the HCN, (Equation 8), 2(HCN) (Equation 9), (HCN + X), (Equation 10), (X), (Equation 11), (XCN), (Equation 12), and (XCN + H), (Equation 13) losses. In these schemes: *X = Cl, Br*, the detected charged fragment is reported in bold whereas the neutral, undetected, fragments are reported in italic. The photoionization efficiency curves of the most prominent fragments were measured and reported in Figure 3 for the 2Cl-pyrimidine and in Figures 1 and 2 in the Supplementary Material for the 2Br- and 5Br-pyrimidine molecules, respectively; the schematic of the investigated fragmentation processes obtained from the calculations are reported in Schemes 1 and 2 for 2Cl- and 5Br-pyrimidine. The scheme of 2Br-pyrimidine is reported in Scheme 3 in the Supplementary Material. Theoretical and experimental results are summarized in Table 1.

### *The Mass Spectra*

In the presentation and discussion of the results, it is important to remember the similarities and differences in the geometrical structure of the three samples among themselves and with respect to the pyrimidine molecule, which can be used as a reference. Indeed, as already mentioned in the previous section and summarized in the photoreactions 7–13, there are equivalent fragmentation channels that can be considered in terms of bond breaking localization. As discussed below, the comparison of these equivalent fragmentation channels, in the light of the theoretical results, provide essential information about the interplay of inductive and resonant effects induced by the halogenation on the pyrimidine ring and their role in governing the dynamics of fragmentation. It is known from previous studies [13–15, 26] that the leading fragmentation channels of the pyrimidine molecule in the VUV energy range are due to the loss of one or two neutral HCN fragments, and the loss of HCN + H leaving the residual $C_3H_3N^+$ (*m/z* = 53), $C_2H_2^+$ (*m/z* = 26), and $C_3H_2N^+$ (*m/z* = 52) charged fragments, respectively (Figure 2a). Equivalent patterns can be identified in the halogenated pyrimidine molecules (photoreactions 8–13).

In Figure 2, the group of peaks at the highest *m/z* values correspond to the parent ions, with their respective isotopic

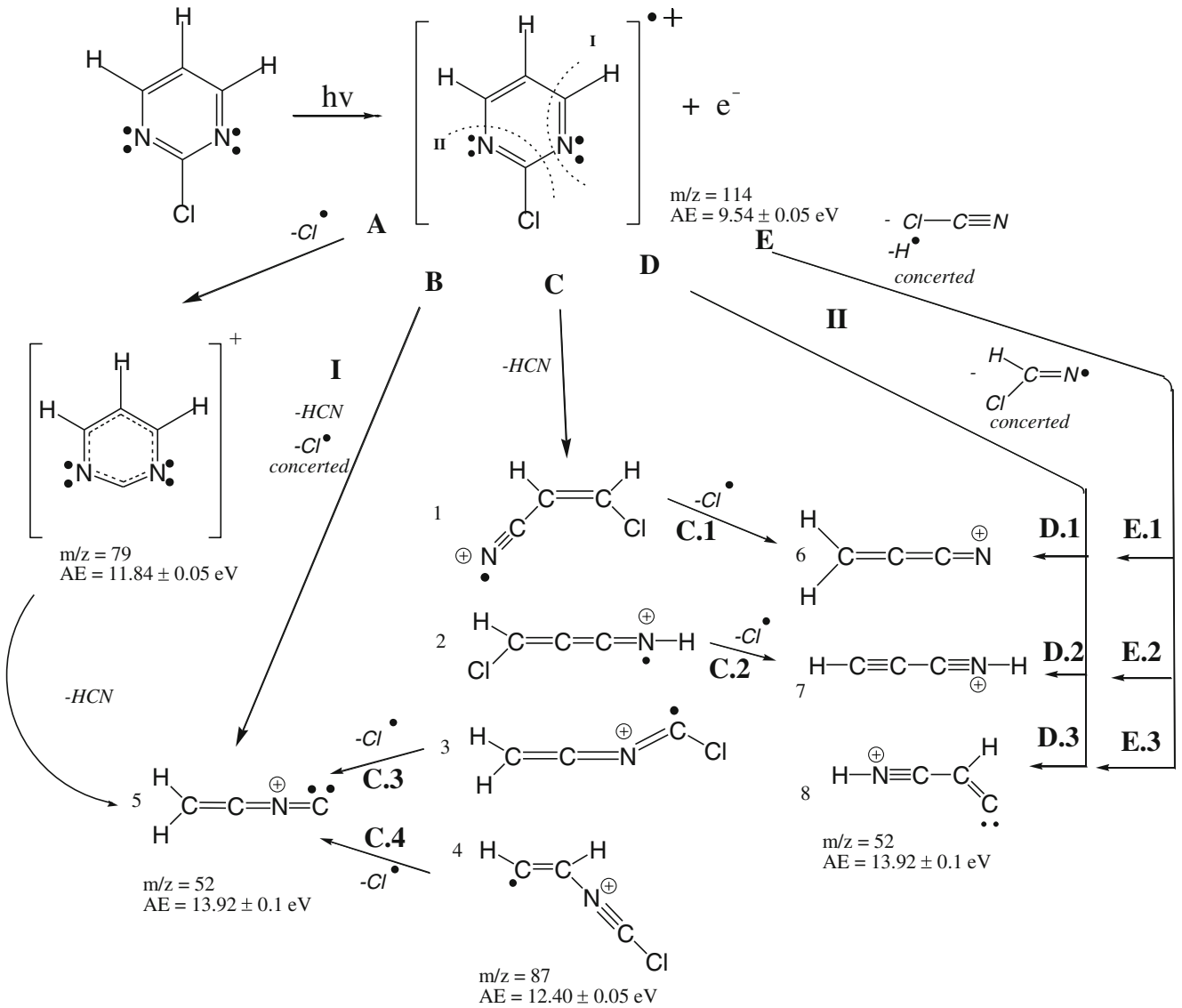


**Scheme 1.** Main fragmentation decay routes of the 2Cl-pyirimidine molecule. The measured values of the appearance energy are given for each fragment. The final geometries of the charged fragment have been labeled with numbers 1–8, whereas the possible fragmentation patterns are labeled with letters A–E. The E.n and D.n ($n$=1, 2, 3) channels correspond to the loss of the H atom bound to C6, C5, or C4 atoms, respectively, after the loss of the ClCN group. The geometries have been optimized at DFT, B3LYP 6-311++G(2d,2p) level using the Gaussian 09 suite of programs [32], and the calculated energies are reported in Table 1

distribution. At 14 eV, they always represent the dominant feature of the spectrum. In the Br-pyrimidine systems, the peaks at $m/z$ = 160 and 158 have almost the same intensity according to the relative abundances of the $^{79}$Br and $^{81}$Br isotopes (50.8 % and 49.2 %, respectively), whereas in the 2Cl-pyrimidine case, the ratio of intensity of the peaks at $m/z$ = 114 and 116 is about a factor 3 due to $^{35}$Cl and $^{37}$Cl isotope ratio (75.77 % and 24.23 %, respectively). The relative abundances of the Br and Cl isotopes are very useful fingerprints for the assignment of specific fragments in the mass spectra. The tiny features observed at 1 u above the parent ions represent the contribution of the $^{13}$C isotope, whose abundance with respect to $^{12}$C is about 1 %.

The fragmentation channel attributable to the loss of a neutral HCN group in pyrimidine may occur via two different but indistinguishable fragmentation pathways. In one case, the process involves the rupture of the C2–N3 and C4–C5 bonds, resulting in an isonitrile form (R−NC see Figure 2). This type of fragmentation is named *channel I* in the following. The other case, named *channel II*, involves the rupture of the N1–C6 and C2–N3 bonds, resulting in a nitrile form (R−CN) (i.e., acrylonitrile). The measurements of six different deuterium-substituted pyrimidines of Milani-Nejad and Stidham [39] show that *channel I* is favored. The fragmentation channel attributable to the loss of a neutral HCN group can be observed also in the halogenated cases

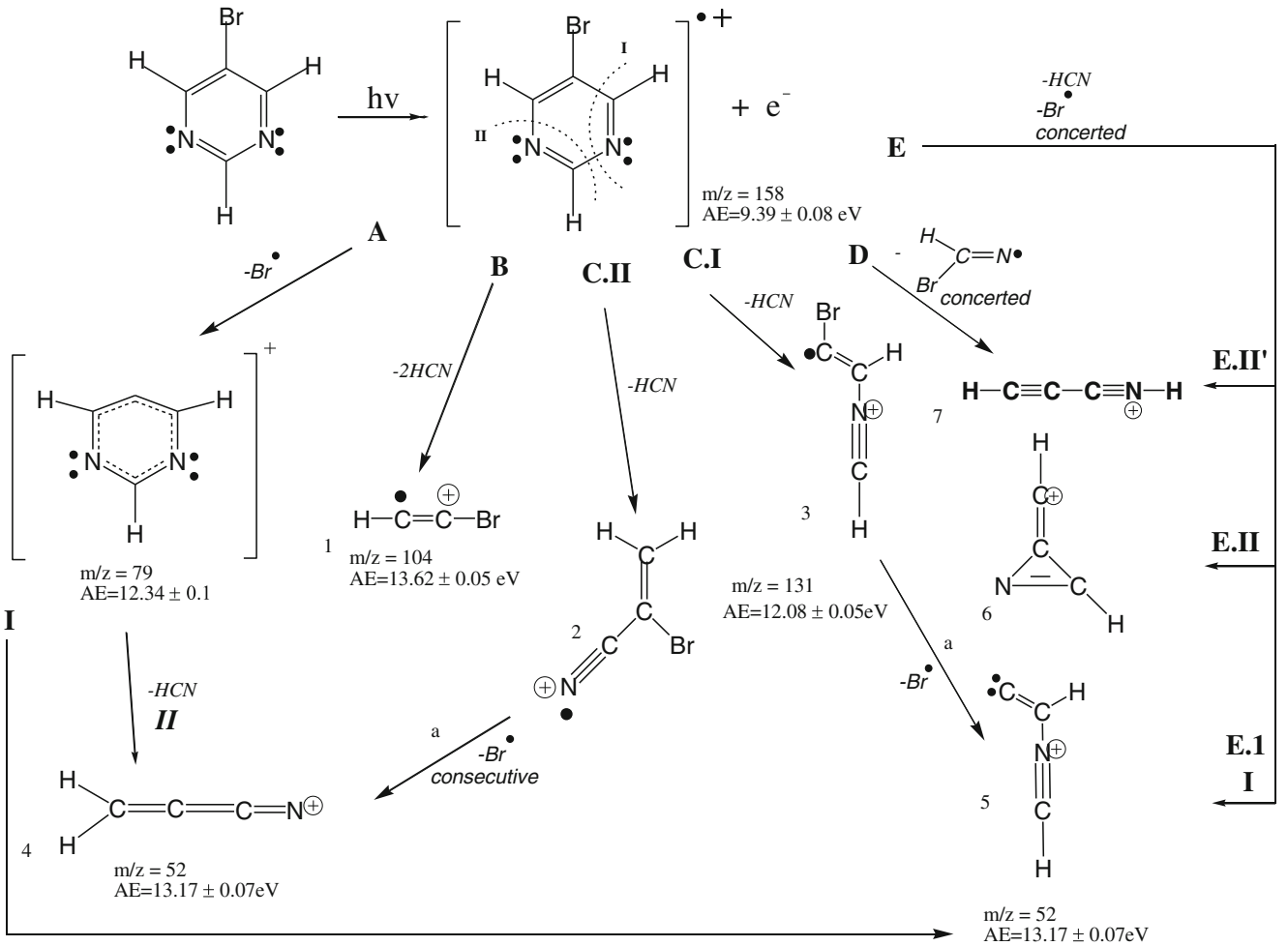


**Scheme 2.** Main fragmentation decay routes of the 5Br-pyrimidine molecule. The measured values of the appearance energy are given for each fragment. The final geometries of the charged fragments have been labeled with numbers 1–7, whereas the possible fragmentation patterns are labeled with letters A–E. For the concerted loss of HCN and Br•, channels I and II have been considered. In the latter case, where the final geometry 6 of the charged fragment has 3-membered ring structure, the N1-C6-C5 angle of the ionized molecule has been forced to 'open', ending up in the linear structure 7. This latter process has been named II′. The difference between D and E processes is whether the neutral HCN and Br• fragments are bound or not. The geometries have been optimized at DFT, B3LYP 6-311++G(2d,2p) level using the Gaussian 09 suite of programs [32]

(photoreaction 8). In the 2Cl- and 2Br-pyrimidine molecules, the position of the halogen atom in site 2 makes the two channels distinguishable. Indeed, *channel I* corresponds to the HCN loss with formation of different radical cations containing Br/Cl atom, respectively (peaks at $m/z = 131/133$ u in the Br-pyrimidines, and 87/89 u in the 2Cl-pyrimidine). On the other hand, *channel II* corresponds to XCN rather than HCN loss, leading to the formation of fragments of $m/z = 53$ in both 2Cl- and 2Br-pyrimidine cases (photoreaction 12).

The channel corresponding to the loss of two HCN groups (photoreaction 9) is observed only in the 5Br-pyrimidine case at $m/z = 104/106$ ($C_2HBr^{+\bullet}$ Figure 2d), whereas it is absent in the 2Br- and 2Cl-pyrimidine cases (i.e., $m/z = 60/62$ for $C_2HCl^{+\bullet}$ Figure 2b). This can be explained by following the previous considerations on the interplay of *channel I* and *channel II* in the HCN loss. Indeed, in the 5Br-pyrimidine the loss of two HCN groups may occur following a combination of *channels I* and *II*, directly leaving a residual halogenated acetylene fragment.

In the pyrimidine mass spectrum the peak at $m/z = 79$, attributable to the loss of the H atom, is barely visible [13]. In the halogenated pyrimidine cases, the same fragment can be attributed to the loss of the neutral halogen atom. In all cases, this will lead to a residual $C_4H_3N_2^+$ (photoreaction 11). In principle, in the Br-pyrimidines, the same $m/z$ value could be also assigned to the $^{79}Br^+$ fragment, corresponding to the complementary process, where the breaking of the C–Br bond leaves the residual charge on the Br atom rather than on the ring. However, the absence of the twin peak attributable to the $^{81}Br^+$ isotope (Figure 2c and d) clearly indicates that this second fragmentation channel, even though dominant in the higher photon energy range [1, 12], can be excluded in the VUV range.

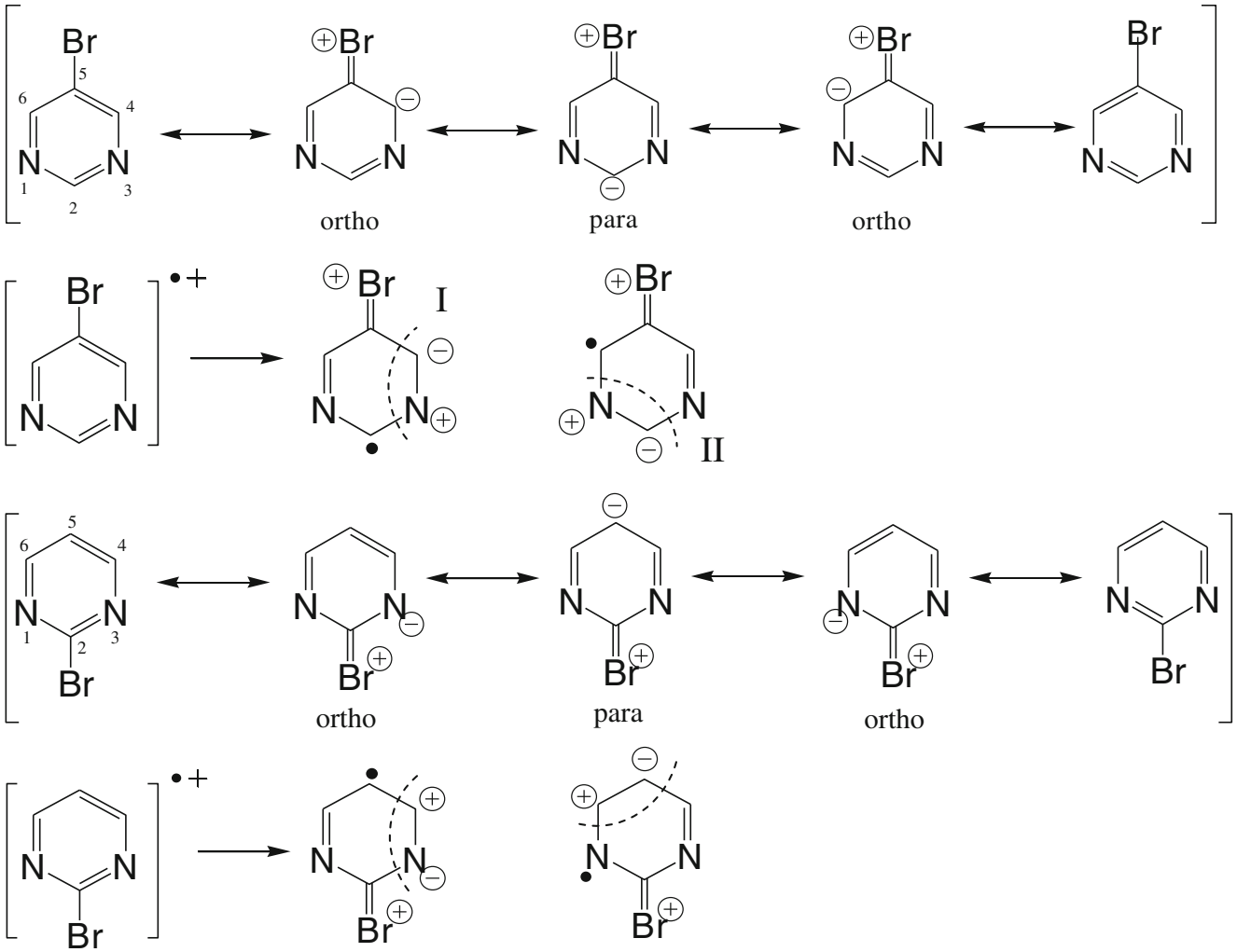


**Scheme 3.** Scheme of the resonance effect in 5Br-pyrimidine and 2Br-pyrimidine responsible of the ejection of the HCN group

The peak at $m/z = 53$, which in the pyrimidine molecule represents the HCN loss, has a correspondence in the halogenated case in the loss of the CN group plus the halogen atom. It is observed only in the 2Cl-pyrimidine mass spectrum where it corresponds to the loss of the ClCN group (photoreaction 12). This may occur via fragmentation *channel II*, with the H atom replaced by Cl in position 2. In the 5Br-pyrimidine case, it is difficult to form this fragment as it would involve a complex rearrangement with a simultaneous/sequential loss of a CN group and the Br atom and, thus, it is unlikely. However, its absence in the case of the 2Br-pyrimidine molecule seems to suggest that the different halogen atoms affect the dynamics of this fragmentation channel. In contrast to the pyrimidine molecule, this seems to be a minor channel in the case of the halogenated molecules. In the works on pyrimidine by Schwell et al. [13], Vall-llosera et al. [21], and Plekan et al. [26], where the incident photon energies are 20, 23, and 21.2 eV, respectively, the intensity of the $m/z = 53$ fragment is comparable to the intensity of the parent ion. The electron impact partial ionization cross-section measurements performed in pyrimidine by Linert et al. [15] show similar trends, with the $m/z = 53$ fragment among the most intense features of the mass spectrum over the full electron energy range, apart from the near threshold region. One possible explanation of the different ratios observed here is that the low photon energy employed (14 eV) corresponds to smaller relative cross-section between the two channels. However, another possibility is that *channel I* is favored with respect to *channel II* for the breaking of the C–C and C–N bonds of the pyrimidinic ring in the case of 2Cl- and 2Br-pyrimidine.

The peak at $m/z = 52$, which in the pyrimidine case is due to the loss of the HCN + H fragments, is observed in all the spectra of the halogenated molecules and corresponds to the loss of the HCN group and the halogen atom (photoreaction 10) or the loss of XCN group and hydrogen atom (photoreaction 13).

In general, the observed branching ratios can be compared among the three spectra taken at the same photon energy and QMS setting (Figure 2b–d), providing some hints on the more likely fragmentation patterns. By comparing, for example, the peaks at $m/z = 79$ and 131/133

(87/89) in the Br- (Cl-) pyrimidine cases we deduce that at the same photon energy, the loss of the halogen atom appears to be more likely with respect to the HCN loss when the halogen atom is in position 2 of the ring, rather than 5.

### *Photoionization Efficiency Curves of 2Cl-Pyrimidine*

The photoionization efficiency curve of the parent ion and the three fragments m/z = 52, 79 and 87 of 2Cl-pyrimidine are shown in Figure 3a–d, respectively, while the principal fragmentation decay paths are shown in Scheme 1. The experimental AEs are collected in Table 1, where they are compared with the calculated values. For the parent ion case, the threshold region is expanded and reported on a log scale in the inset of Figure 3a, in order to illustrate the data analysis procedure described above.

For the parent ion, the measured IE value of 9.54 ± 0.05 eV is consistent with the calculated value of 9.61 eV, and lower than the experimental determination of 9.84 ± 0.02 of the $6b_2(n_{N-})$ ground electronic state of 2Cl-pyrimidine measured in photoelectron spectroscopy [16]. This difference can be explained considering that the photoelectron spectroscopy provides vertical ionization energies and depends on the Franck–Condon overlap between the involved states, whereas the experimental IE determines the onset of the ion signal. Furthermore the theoretically predicted AE (11.92 eV) for the *m/z* = 79 fragment (process A) is also in good agreement with the experiment (11.84 ± 0.05 eV). In both cases, the final state of the reaction is relatively simple, with the unbroken molecule or the loss of the halogen atom, respectively. Further considerations will be needed in the case of the *m/z* = 87 and 52 fragments, where several scenarios can, in principle, arise.

As discussed in the previous section, only *channel I* can contribute to the *m/z* = 87 (AE = 12.40±0.05 eV) fragment (process C) in the 2Cl-pyrimidine case. In the calculations, we considered several possible geometries for the residual $C_3H_2NCl^{+\bullet}$ fragment and computed their enthalpies of formation. The resulting four lowest geometries, labeled 1 to 4 in order of increasing energy, are reported in Scheme 1. Structure 4 is obtained in the DFT calculation by removing the C4, N3 atoms as well as the H atom bound to C4. In this way, no rearrangement or isomerization of the parent ion structure before the fragmentation nor of the residual charged fragments after the fragmentation is needed. The computed energy for structure 4 (12.35 eV) is consistent with the measured AE value within the experimental error. The other structures are obtained by isomerization. Structure 1 is the lowest in energy; therefore, this geometry appears to be the most stable, as already proposed by Schwell et al. [13] for the HCN loss in pyrimidine. Indeed, the calculated AEs of structures 1, 2, and 3 are lower than the experimental value, and transition from one to another requires a molecular rearrangement (i.e., the formation of transient species with barriers to overcome). In the present case, the calculated barriers between the four configurations of the $C_3H_2NCl^{+\bullet}$ fragment, labeled 1–4 in Scheme 1, are all larger than 1 eV, as shown in Figure 3 of the Supplementary Material.

The values of the calculated energy barriers are too high to explain the transition from the most likely structures 4 or 3 to the energetically more favorable structures 1 and 2 of the fragment. The proximity of the theoretical AE of fragment 4 to the experimentally measured AE may suggest that such a stable geometry is formed in the threshold region and as long as there is not enough energy to overcome the barrier towards more stable geometries. In light of these considerations, we assign the structure 4 to the $C_3H_2NCl^{+\bullet}$ fragment (*m/z* = 87).

The *m/z* = 52 fragment is assigned to the residual $C_3H_2N^+$ ion after the HCN and Cl loss (or ClCN and H loss). The experimental AE value is 13.92 ± 0.10 eV. This is a challenging case for the theoretical calculations. This fragment indeed may be obtained either by concerted (processes B, D, and E) or sequential (processes A and C) reactions. Moreover, different geometrical structures of the charged- (structures 5–8) and neutral fragments can be involved (see Scheme 1). We begin treating the loss of HCN and Cl radical. This may happen in a simultaneous or a sequential way. From the theoretical point of view, in the first case (process B) the HCN group and the Cl atom are removed simultaneously from the neutral molecule; then the geometry of the fragment is re-optimized and its enthalpy of formation computed. The sum of the enthalpies of formation of the two separated neutral fragments HCN and Cl·, according to formula 4, gives the AE of 14.79 eV (Table 1) much higher than the experimental determination of 13.92 ± 0.10 eV. This mechanism is related to *channel I* of HCN loss. In the sequential process, the loss of the halogen atom may precede (process A) or follow (process C) the loss of the HCN group. In both cases, the geometry of the intermediate fragment obtained by removing the first species is re-optimized before removing the second one. In the latter case, process C, the first step coincides with the formation of the *m/z* = 87 and has already been discussed in this section. The subsequent Cl loss from fragments in structures 1–4 leads to structures 5, 6, or 7, depending upon the intermediate state.

Another possible scenario implies the loss of the ClCN group and a hydrogen atom (processes D and E) in a concerted or sequential way proceeding through *channel II*. Several sequential cases (see Schemes 1 and 2 of the Supplementary Material) have been considered in the theoretical calculation, including the loss of each one of the three possible H atoms preceding/following the ClCN loss and the possibility of formation of both the HCNCl· or ClCN + H· neutral fragments. Most of these sequential patterns following *channel II* end up in similar final states as their equivalent concerted reactions, and others give three carbon ring sterically hindered structures with correspondingly higher AE. For these reasons, we discarded the

**Table 1.** Experimental and Theoretical Values of the Halogenated Pyrimidine Appearance Energy and Fragmentation Products

| **Channels** | | | **2Cl-pyrimidine** | | | | **2Br-pyrimidine** | | | | **5Br-pyrimidine** | | | |
|---|---|---|---|---|---|---|---|---|---|---|---|---|---|---|
| *m/z* | *Possible fragment cation* $mi^+$ | *Neutral fragments* | $AE_{exp}$ (eV) | $AE_{G3B3}$ (eV) | | | $AE_{exp}$ (eV) | $AE_{G3B3}$ (eV) | | | $AE_{exp}$ (eV) | $AE_{G3B3}$ (eV) | | |
| | | | | *Geometry* | $AE_{298K}$ | *Process* | | *Geometry* | $AE_{298K}$ | *Process* | | *Geometry* | $AE_{298K}$ | *Process* |
| (parent ion) | | | 9.54±0.05 | | 9.61 | (IE) | 9.50±0.05 | | 10.00 | (IE) | 9.39±0.08 | | 9.91 | (IE) |
| 87 (2Cl-pyr) | $C_3H_2NX^{+\bullet}$ | HCN | 12.40±0.05 | 1. | 11.65 | C | 12.52±0.05 | 1. | 11.45 | C | 12.08±0.05 | 3. | **11.96** | C.I |
| 131 (2Br-,5Br-pyr) | | | | 2. | 11.64 | C | | 2. | 11.48 | C | | 2. | 11.66 | C.II |
| | | | | 3. | 12.25 | C | | 3. | 12.06 | C | | | | |
| | | | | 4. | **12.35** | C | | 4. | 12.20 | C | | | | |
| | | | | | | | | 9. | **12.41**[b] | C | | | | |
| 104 | $C_2HX^{+\bullet}$ | 2HCN | — | — | — | — | | — | … | — | 13.62±0.05 | 1. | **13.42** | B |
| 79 | $C_4H_3N_2^+$ | $X^{\bullet}$ | 11.84±0.05 | | **11.92** | A | 11.06±0.05 | | **11.27** | A | 12.35±0.10 | | **12.33** | A |
| 52 | $C_3H_2N^+$ | HCN + X | 13.92±0.10 | 5. | 14.79 | A/B/C.3/C.4 | 13.60±0.10 | 5. | 14.15 | A/B/C.3/C.4 | 13.17±0.07 | 4. | **13.66** | A.II/C.IIa |
| | | | | 6. | 14.33 | C.1 | | 6. | **13.69** | C.1 | | 5. | 15.08 | E.I/C.Ia/A.I |
| | | | | 7. | 12.65 | C.2 | | 7. | 12.01 | C.2 | | 6. | 14.70 | E.II |
| | | | | | | | | 10. | 14.34[b] | C.5 | | 7. | 11.97 | E.II′ |
| | | $HCNX^{\bullet}$ | | 6. | 14.04 | D.1 | | 6. | 13.92 | D.1 | | 7. | 12.20 | D |
| | | | | 7. | 12.36 | D.2 | | 7. | 12.23 | D.2 | | | | |
| | | | | 8. | 14.71 | D.3 | | 8. | 14.59 | D.3 | | | | |
| | | $XCN + H^{\bullet}$ | | 6. | 15.36 | E.1 | | 6. | 15.25 | E.1 | | … | … | … |
| | | | | 7. | **13.68** | E.2 | | 7. | **13.56** | E.2 | | … | … | … |
| | | | | 8. | 16.03 | E.3 | | 8. | 15.91 | E.3 | | … | | |

[a]Theoretical AE corresponding to the proposed fragmentation paths are in bold
[b]The structures of these fragments are shown in Scheme 3 in the SM

sequential paths, suggesting that from the energetic point of view, a concerted reaction is favored. This leads to the structures 6, 7, or 8, depending on which H atom is removed.

It is important to remember that in the present calculation the values of the AE depend not only on the geometry of the charged fragment, but also on the structure of the neutral fragments and, therefore, to some extent on the fragmentation mechanism. So, for example, the appearance energies of processes C.1, D.1, and E.1 are all different although they end up with the same structure of the charged fragment, whereas the computed AEs of processes A, B, C.3, and C.4 are all the same and are, therefore, indistinguishable. This of course refers only to the adiabatic AE calculated according to Equations 3 and 4 while most likely there will be energy barriers to overcome not included in the present calculations. These results have been summarized in Table 1, where both the theoretical AE and the corresponding geometries and reaction mechanisms are reported.

The calculated AE for the charged fragment in geometry 5 is too high (14.79 eV) compared with the experimental value, so the fragmentation pathways A, B, C.3, and C.4 can be discarded. A similar conclusion applies to the pathway E.3, E.1, D.3, and C.1 with calculated AE of 16.03 eV, 15.36 eV, 14.71 eV, and 14.33 eV, respectively. Mechanisms E.n and D.n ($n$=1, 2, 3) of *channel II* type and leading to structures 6–8 differ only by the H atom lost. In these cases, the linear structure 7 is obtained by forcing the input geometry to have the N1-C6-C5 angle larger or equal to 133°, which is greater than the equilibrium value of 122.48° for the neutral molecule. This would imply the existence of a reverse barrier for the formation of an activated complex with this larger angle preceding fragmentation. The overcoming of the barrier can explain the 0.24 eV difference between the measured and calculated AE values. As already mentioned, the calculations do not take into account the energy of the barrier, giving a theoretical AE lower than the experimental one. In the case where the linear structure 7 is formed in a sequential process from *channel I* via structure 2, (process C.2), no angle straining is needed. In this case, an AE value lower than the experimental one is obtained. In principle, this energy difference could be due to the need to overcome the potential barrier from structure 4 to 2 (see Figure 3 in the Supplementary Material). However, the value of the calculated barrier of 1.83 eV is not consistent with the difference of 1.27 eV between the experimental and calculated AE for path C.2. We thus suggest that the most probable path is E.2, which gives the nearest AE value to the experimental one. Pattern E.2 corresponds to the concerted loss of ClCN + $H^{\bullet}$, involving the H atom bound to C5. The molecular rearrangement leading to the formation of the neutral $HClCN^{\bullet}$ radical with the migration of an H atom bound to the C4, C5, and C6 atoms, respectively, may occur too, via processes D.1 to D.3. As already noted by Schwell et al. [13], in the pyrimidine case the loss of $H_2CN$ or its isomer HCNH are less probable because these radicals involve more endothermic reactions and, moreover, their formation would require rearrangement of at least one H atom. So this pattern, although leading to more stable fragments, will probably require significant energy barriers to overcome.

## *Photoionization Efficiency Curves of 2Br-Pyrimidine*

The photoionization efficiency curves of the parent ion and of the three fragments, $m/z$=52, 79, and 131 of 2Br-pyrimidine are shown in Figure 1a–d in the Supplementary Material, whereas the experimental and theoretical AEs are collected in Table 1. A schematic of the considered fragmentation pattern is sketched in Scheme 3 in the Supplementary Material. Apart from the replacement of the Cl with a Br atom, the 2Br-pyrimidine molecule presents many similarities with the 2Cl-pyrimidine as, for example, the optimized geometrical structures of the different fragments and the possible fragmentation paths.

The experimental IE=9.50±0.05 eV for the parent ion is lower than the vertical ionization potential of the $5b_2(n_{N-})$ ground state of 2Br-pyrimidine ion, 9.93±0.02 eV [16], measured in photoelectron spectroscopy. The calculated IE value of 10.00 eV is about 0.5 eV higher than the experimental IE and higher than the vertical ionization potential. Considering that the calculated IEs give the adiabatic thresholds, whereas the ground electronic state corresponds to a vertical transition, this larger value of the theoretical IE with respect to the experimental one is likely due to the basis set used in the G3B3 calculation, which does not include *g*-type polarization functions to the G3 large basis set for the elements beyond Al. Indeed, also the vertical ionization potential calculated by O'Keeffe et al. using the P3 calculation with the 6-311G(2df,2p) basis augmented by the SDD basis set gives a value [16] that is higher than its corresponding experimental value.

The difference between the calculated and measured AE values decreases to about 0.21 eV in the case of the $m/z$=79 fragment ($AE_{exp}$=11.06±0.05 eV), corresponding to the loss of the neutral Br atom. As for the parent ion case, a higher theoretical value can be similarly attributed to the lower level of accuracy of the present theoretical approach in the presence of the heavy Br atom in the molecule.

The HCN loss in 2Br-pyrimidine can proceed only through *channel I*, producing the fragment at $m/z$ = 131. Its measured AE value is 12.52 ± 0.05 eV (process C in Scheme 3, Supplementary Material). According to the B3LYP predictions, the $C_3H_2NBr^{+\bullet}$ charged fragment may exist in several geometries that have been labeled 1–4 and 9 in Scheme 3 (Supplementary Material) by increasing energy. Structures 1–4 are equivalent to the 2Cl-pyrimidine case (Scheme 1). Structure 9, the one with the highest enthalpy of formation among the five, is a four-membered ring structure obtained in a DFT calculation by the rupture of the C2–N3 and C4–C5 bonds without any isomerization. Within the uncertainty of the present AE calculations, this is the most

similar to the experimental value and is considered to be the most probable structure obtained during this fragmentation. Interestingly, the equivalent computational procedure in the 2Cl-pyrimidine case does not lead to a ring structure. The results are confirmed by performing a B3LYP calculation employing the 6-311G(2df,2p) larger basis set augmented by the SDD basis set for both cases of Br or Cl. Similar to the case of 2Cl-pyrimidine, the values of the potential energy barriers between two structures in the series 1–4 are always larger than 1.3 eV (see Figure 4 in the Supplementary Material). Thus, it does not seem to be possible to overcome such barriers to access the more stable structures 1–4.

The $m/z = 52$ peak is assigned to the $C_3H_2N^+$ fragment (AE = 13.60 ± 0.10 eV) and may be formed either in a concerted (processes B, D, and E in Scheme 3, Supplementary Material) or in a sequential (processes A and C) reaction. The corresponding AEs are reported in Table 1. Such fragmentation mechanisms have been described in detail in the case of the 2Cl-pyrimidine molecule, so they will be discussed very briefly here. In the concerted reaction, the opening of the ring with the simultaneous release of the bromine atom and the HCN group via *channel I* leads to structure 5 (process B). The other channel, *channel II*, which involves the loss of the BrCN group and an H atom, leads to structures 6, 7, or 8, depending on the position of the H atom (processes D and E). The difference between processes D and E consists in the neutral complementary fragment, which can be formed by one or two separated moieties. Considering that the enthalpy of formation of $HCNBr^{\bullet}$ is smaller than HCN + $Br^{\bullet}$, the corresponding adiabatic AE for process D is smaller than for process E. Nevertheless, the D pattern will require molecular rearrangement, increasing the effective appearance energy of the ion formed in this particular path. In the sequential reaction, the loss of the $Br^{\bullet}$ radical may precede (process A) or follow (process C) the loss of the HCN group. In the latter case, structure 5 is formed from the intermediate structures 3 and 4, whereas the loss of the halogen atom from fragments 1 and 2 leads to structures 6 and 7.

As in 2Cl-pyrimidine, also in 2Br-pyrimidine structure 5 is characterized by a too high adiabatic AE value with respect to the experimental one and, therefore, paths A, B, C.3, and C.4 were discarded. The absence of the peak corresponding to the $m/z = 53$ fragment (attributable to the BrCN loss) in the mass spectrum of Figure 2c makes it unlikely that process E occurs sequentially. However, this does not exclude that it could occur in a concerted manner with the simultaneous loss of the BrCN group and H atom (E.2 path with AE = 13.56 eV). In contrast to 2Cl-pyrimidine, in the case of 2Br-pyrimidine we have also to consider the sequential loss of the HCN group and the $Br^{\bullet}$ radical (i.e., path C.1 leading to structure 6 with AE = 13.69 eV). These two paths are close in energy to the experimental value (AE = 13.60 ± 0.10 eV). Therefore, we conclude that in 2Br-pyrimidine, the consecutive (−HCN, $-X^{\cdot}$) and concerted (−XCN, $-H^{\bullet}$) processes are competitive, unlike the 2Cl-pyrimidine case, where the concerted ClCN and $H^{\bullet}$ loss is dominant in the formation of the fragment at $m/z = 52$. This is due to the different electronegativity of the Br atom with respect to Cl, which makes possible the rupture of Br−C bond at lower energy.

## *Photoionization Efficiency Curves of 5Br-Pyrimidine*

In 5Br-pyrimidine, the fragmentation patterns show significant differences with respect to the 2Cl- and 2Br-pyrimidine cases because of the different halogen atom and its different location. The partial photoionization efficiency spectrum of the parent ion and the four ionic fragments $m/z = 52$, 79, 104 and 131 are shown in Figure 2 in the Supplementary Material, whereas the experimental AEs, together with the calculated values, are collected in Table 1. In Scheme 2, the investigated fragmentation paths of this molecule are sketched.

For the parent ion, the G3B3 method overestimates the experimental IE (9.39 ± 0.08 eV) by about 0.5 eV. As already discussed in the case of the 2Br-pyrimidine, this discrepancy can be attributed to the presence of the Br atom with a consequent reduced accuracy of the G3B3 calculation. Indeed, the experimental value, 9.39 ± 0.08 eV, is significantly lower than the measured vertical ionization potential of this molecule, at 9.93 ± 0.02 eV [16]. As for the 2Br-pyrimidine case, the vertical ionization potential calculated by O'Keeffe et al. [16] using a similar computational analysis, the P3 calculation with the 6-311G(2df,2p) basis augmented by the SDD basis set, gives a value that is higher than the corresponding experimental one.

The loss of the radical halogen atom, $Br^{\bullet}$, leads to the $m/z = 79$ fragment (process A in Scheme **2**). In this case, the theoretically predicted AE (12.33 eV) is in good agreement with the experiment (12.35 ± 0.10 eV). This could be explained in the $m/z = 79$ case, if the computed enthalpy of formation of the charged fragment, which does not contain the Br atom, is likely to be more accurate.

The $m/z = 104$, attributed to the halogenated acetylene cation, is due to the loss of two HCN groups (see process B in Scheme 2). The equivalent channel in pyrimidine is achieved by a combination of *channels I* and *II*, and is not observed in the 2Cl- and 2Br-pyrimidine cases, where the halogen atom in site 2 locks the loss of HCN via *channel II* and makes the formation of the halogenated acetylene very unlikely. This is, instead, a quite straightforward process when site 2 is occupied by an H atom, as in the pyrimidine or 5Br-pyrimidine cases. The calculated and measured AEs agree with each other, assuming a reverse energy barrier. A process in which this cation is formed via the loss of $N_2$ and $C_2H_2$ from the parent cation has been also considered. As observed by Schwell et al. [13] in the case of pyrimidine, this scheme is thermodynamically allowed, but it is kinetically less probable because of the required rearrangement to form $N_2$.

The previous considerations established that in 5Br-pyrimidine both *channels I* and *II* involving the loss of the HCN group are active. Each one of the two channels leads to the same $m/z = 131$ fragment, although with different final geometries (see structures 3 and 2 for paths C.I and C.II, respectively, in Scheme 2) and, therefore, different computed AEs (see Table 1). The calculated AE for path C.II, corresponding to *channel II* and leading to structure 2, is lower than the one for path C.I. (i.e., *channel I*, leading to structure 3). So, from the energetic point of view structure 3 is less stable than structure 2. However, structure 3 can be reached from the parent ion by removing directly the N1, C2 atoms and the H atom in position 2 and re-optimizing the structure, whereas structure 2 requires isomerization ( i.e., the overtaking of energy barriers). Furthermore, the calculated AE of path C.I is in closer agreement with the experimental result. For these reasons, the fragmentation channel C.I appears to be more likely.

The situation is more complex for the $m/z = 52$ fragment (−HCN –Br), where both *channels I* and *II* as well as the concerted (processes D and E) and sequential reactions with Br loss following (C.IIa, C.Ia) or preceding (A) the HCN loss have been considered. All of these possibilities are summarized and sketched in Scheme 2, whereas the corresponding computed AEs are reported in Table 1. Structure 6 can be obtained by the concerted loss of the HCN group in *channel II* and the Br· radical. However this geometry is quite unstable because of the high tension of the three atom rings. Structure 5, obtained either from a sequential or a concerted reaction with the loss of the HCN group in *channel I* and the $Br^{\bullet}$ radical, is even more unstable than structure 6 so that their corresponding adiabatic AE values are higher than the experimental one. Therefore, processes C.Ia, A.I, E.I, and E.II can be discarded. The linear structure 7 for the $C_3H_2N^+$ fragment can be formed via the D and E.II′ processes. This may occur via the concerted loss of the HCN group in *channel II* and the $Br^{\bullet}$ radical and then forcing the N1-C6-C5 angle to become larger than its equilibrium value of 121.31° to prevent the closing of the ring that would lead to structure 6. We discard the linear structure because of the high reverse barrier of about 1.2 eV (difference between the experimental and theoretical value), which would lead to an activated complex very disadvantageous by the steric hindrance of the bromine atom, which makes the stretching of the angle difficult. The difference between the D and E processes is whether the neutral HCN and $Br^{\bullet}$ fragments are bound or separated. Their respective AEs are shifted by 0.23 eV [i.e., with the former (process D) having a higher AE than the latter (E process)]. Therefore, the two separated neutral fragments are in a thermodynamically favorable condition. This is also reinforced by the fact that the production of the HCNBr· radical (process D) requires the migration of the bromine atom, an endothermic reaction most likely involving some energy to overcome potential barriers. Finally let us consider structure 4. It can be reached in a sequential reaction via paths A.II and C.IIa with the $Br^{\bullet}$ loss, respectively, preceding or following the loss of the HCN group in *channel II*. The computed AE of 13.66 eV for $m/z = 52$, not far from the experimental measurements, suggests that this fragmentation channel proceeds via the sequential loss of the HCN and $Br^{\bullet}$ fragments.

## *The Substituent Effect*

In the previous sections, the experimental and theoretical results of the study of the appearance energy of the most prominent fragments of three halogen substituted pyrimidine molecules were presented and discussed. More information about the fragmentation dynamics of this class of molecules can be gathered by comparing the results obtained for equivalent fragmentation channels of the three selected targets and the unsubstituted pyrimidine molecule. The 2Cl-, 2Br-, and 5Br-pyrimidine molecules allow the effects of the different halogen substitution (Cl or Br in the 2Cl- and 2Br-pyrimidine, respectively) and the site of halogenation (2 or 5 for the 2Br- and 5Br-pyrimidine, respectively) on the fragmentation dynamics of the pyrimidinic ring to be investigated. With this in mind, the AE of the main fragments and the corresponding proposed geometrical structure/fragmentation mechanisms are discussed in this section.

In the case of the parent ion (photoreaction 7), the measured AE of the three molecules are very similar to each other and to that of the unsubstituted pyrimidine molecule. The average value is about 9.48 eV [15, 16]. As already observed by other authors for the cases of aminoacids and DNA/RNA bases [40 and references therein], this can be explained by the fact that the highest occupied molecular orbital (HOMO) in these molecules is often the nitrogen lone pair orbital. The simplicity of the photoreaction, which leads to the parent ion with just the singly ionized, unbroken, molecule in the final state offers the most straightforward way for a comparison of the experimental and theoretical values of the AE. There is a good agreement for the 2Cl-pyrimidine, but significant discrepancies have been observed in the brominated cases, with the theoretical values exceeding the experimental values by about 0.5 eV. Considering that the present computational approach gives the adiabatic threshold (i.e., the minimum energy required for the selected process to happen), one should expect the experimental values to be larger than the calculated ones. However, the observations that (1) the measured AE values for the parent ions are consistently lower that the respective vertical ionization energy independently measured in photoelectron spectroscopy by O'Keeffe et al. [16], whereas the calculated values are similar or even larger, and (2) similar discrepancies have been observed by the same authors in the comparison between experimental and theoretical results obtained using the P3 calculation with the 6-311G(2df,2p) basis set for the vertical ionization potential of the 2Br- and 5Br-pyrimidine molecules, seem to support the experimental

findings. The quality of the calculation in the case of the other fragments, where more than one structure is possible both for the neutral and charged fragments, is more difficult to assess and the possibility of systematic differences between experimental and theoretical results is something to be aware of in the comparison.

In the photon energy range investigated in the present work, the loss of the HCN group (photoreaction 8) seems to be more probable than the loss of the halogen atom (photoreaction 11) in the 5Br-pyrimidine, whereas the opposite occurs in the 2Cl- and 2Br-pyrimidine molecules. This can be observed in the mass spectra of Figure 2, as well as in the measured AE of the corresponding channels reported in Table 1. In Figure 2, the measured branching ratio of fragments with *m/z* 131/79 is >>1 in 5Br-pyrimidine and<<1 in 2Br-pyrimidine (as well as in 2Cl-pyrimidine where *m/z* 87/79 is<<1). The charged fragment of the HCN loss channel has AE(5Br-pyrimidine)<AE(2Cl-pyrimidine)<AE(2Br-pyrimidine), showing that the HCN loss is thermodynamically favored in 5Br-pyrimidine, whereas the halogen loss becomes more likely in the other two cases. This suggests that a dominant role is played by the site of halogenation rather than the specific halogen atom. Indeed, the halogen atom acts on the electronic structure of the pyrimidine derivatives, as well as in most aromatic compounds, via two main mechanisms, the inductive and the resonance effects [16, 20]. The former is due to the electronegativity of the halogen substituent, which withdraws electron density from the ring, whereas the latter is due to conjugation between the lone pair orbitals of the halogen atom and the π orbitals of the ring. In a resonance structure description of such an effect, the halogen carries a positive charge, while giving electronic charge to the aromatic system, thus forming a double bond with its C neighbor. The negative charge can be considered to be preferably localized on ortho and para positions with respect to the halogen. We suggest that our observation is probably due to the more relevant role played by the resonance compared with the inductive effect when the halogen atom is in position 5 rather than 2. In 5Br-pyrimidine, when the parent ion is formed one could imagine two possible scenarios, schematized in Scheme 3. On one hand, when there is an activation of the ring in "ortho" position, the N3–C4 bond becomes stronger with respect to the N3–C2 and C4–C5 bonds, thanks to the covalent and ionic nature of the bond. This makes more likely the rupture of the nearest bonds with a sequential release of the HCN group following *channel I*. On the other hand, when there is activation in "para" position, the N1–C2 bond becomes stronger compared with the nearest ones. In this case, the release of the HCN group will happen via *channel II*. These effects can explain the formation in 5Br-pyrimidine of the intense peaks at *m/z*=131 (due to HCN loss via either *channel I* or *II*) and 104 (due to the loss of two HCN groups via the joint action *channel I* and *II*). The situation is different when the halogen atom is bound to the C2 atom, where the same para-ortho activation leads to the HCN release via *channel I* (ortho activation) or $C_2H_2$ release (para activation). This simple picture only takes into account the site of halogenation of the pyrimidine ring to explain the experimental observation of efficient release of HCN in the case of halogenation in site 5. On the other hand, in 2Cl- and 2Br-pyrimidine the most likely fragmentation channel is the loss of the halogen atom, attributable to a more relevant inductive effect when the halogen atom is in position 2, surrounded at close range by two nitrogen atoms.

As already discussed, both *channels I* and *II* are available in the 5Br-pyrimidine case for the HCN loss, whereas only *channel I* is possible in the 2Cl- and 2Br-pyrimidine. Therefore, the present experimental observations could be interpreted in the light of a preferred mechanism like *channel I* for the HCN loss and the breaking of the pyrimidinic ring. This explanation is consistent with the results of mass spectrometric studies of pyrimidine and a set of deuterated pyrimidines [39], which suggest that the loss of HCN involves mainly the C4 carbon atom rather than the C2 one. On the other hand, this explanation would be in contrast with the suggestion of Schwell et al. [13], who associates the residual $C_3H_3N^{+\bullet}$ fragment of pyrimidine to the acrylo-nitrile form, which can be produced only by *channel II.* It should be noted however that Schwell et al. [13] left the question open. In the present work, the HCN loss proceeding via *channel II* in the 5Br-pyrimidine case leads to a more stable structure for the $C_3H_2NBr^+$ fragment, even though this requires a molecular rearrangement, whereas a better matching between theoretical and experimental AE values is observed considering the fragmentation via *channel I.* Thanks to the computational analysis performed, we are able to assign a specific geometry and fragmentation pathway to each cation fragment. In the case of 5Br-pyrimidine, our results suggest that the most favorable path for the HCN loss is through *channel I.* This is also consistent with the resonance schematic of Scheme 3, where the ortho limit structures have the major contribution to the hybrid structure (thanks to the symmetry of the molecule) favoring the corresponding fragmentation *channel I.*

Consistently with the arguments explained above, the −2(HCN) channel (photoreaction 9) has been observed only in the 5Br-pyrimidine molecule, where a combination of *channels I* and *II* can directly lead to the observed residual halogenated acetylene cation. This observation confirms that both channels are active.

It is important to clarify at this stage that *channel II* cannot exist as an HCN loss channel when the halogen atom is in position 2, although it can still be considered in the opening of the ring via the breaking of the C2–N3 and N1–C6 bonds. In this case, it leads to XCN loss (X = Cl, Br) and, therefore, to a different *m/z* fragment (*m/z* = 53) with respect to those attributable to HCN loss. The *m/z* = 53 fragment is not observed in 5Br-pyrimidine, as this would imply a very significant molecular rearrangement with

respect to the neutral molecule; it is observed in 2Cl-pyrimidine but not in 2Br-pyrimidine. This is due to the fact that the chlorine atom is more electronegative than nitrogen, which is, in turn, more electronegative than bromine (Cl > N > Br > C). This different atom's electronegativity is the key to explain the relative contribution of photoreaction 11 (−X) and 12 (−XCN) in 2X-pyrimidines when X = Cl or Br. Indeed, the Cl atom can weaken the C–N bond more efficiently than the Br atom, making the ClCN loss possible and competing with the loss of Cl radical. On the other hand, the Br atom (which is less electronegative than the two nearest N atoms), can weaken the X–C bond favoring the release of the Br radical more than the BrCN group. As in the HCN loss channel the dominant role was played by the site of halogenation, in the case of the XCN channel the most relevant role is played by the particular halogen atom (see Figure 5 in the Supplementary Material). This simple explanation based on the atom electronegativity is supported by the halogen loss channel, which is more intense when the halogen atom is in position 2 rather than 5, where the C2–X bond is weakened by the presence of the nearby N atoms in positions 1 and 3, and definitely enhanced in the case of the 2Br-pyrimidine.

The cation fragment in photoreactions 10 and 13 corresponds to $m/z = 52$. As reported in Table 1 and in Schemes 1 and 2 (and Scheme 3 in the Supplementary Material) the description of this channel is quite complex, and several scenarios can arise. Summarizing the results of Table 1, in all cases the formation of the $HCNX^{\bullet}$ fragment is not favored according to energy considerations, whereas two separated fragments have a more stable configuration. These neutral fragments could be HCN and $X^{\bullet}$ (photoreaction 10) or XCN and $H^{\bullet}$ (photoreaction 13). From a theoretical point of view, although in the 2Cl-pyrimidine the proposed fragmentation mechanism is a concerted reaction leading to the release of the ClCN neutral fragment and a $H^{\bullet}$ radical, in the 2Br-pyrimidine both processes may happen, even though in different ways: concerted BrCN and $H^{\bullet}$ loss or sequential HCN and Br loss. Considering the larger uncertainty of the theoretical calculation in the brominated cases, we leave both options open considering the two channels competitive. In the case of 5Br-pyrimidine the proposed mechanism is a sequential process with the release of a Br· radical and a neutral HCN group proceeding via *channels II*. This implies that in the chlorinated case, the free radical is $H^{\bullet}$, whereas in the brominated cases, particularly 5Br-pyrimidine, the free radical is $Br^{\bullet}$.

## Conclusions

The halogenated pyrimidines constitute an important class of prototype radiosensitizing molecules and, therefore, the study of their fragmentation dynamics is of interest to understand the fundamental mechanisms of the enhanced radiation damage when these molecules are selectively incorporated in the DNA of tumor cells. The IE of the parent ion and the AE of some selected fragments of 2Cl-, 2Br- and 5Br-pyrimidine molecules have been measured and calculated, the possible fragmentation pathways have been discussed, and the role played by the halogen atom and/or site of halogenations have been unraveled. For the parent ion case, the experimental IE values are all very similar to that of pyrimidine because in all of these cases the highest occupied molecular orbital is the nitrogen lone pair. The HCN loss channel is found to be favored with respect to the halogen radical loss channel in the 5Br-pyrimidine case, whereas the opposite occurs in the case of the 2Cl- and 2Br-pyrimidine molecules. The 2(HCN) loss is only observed in the 5Br-pyrimidine. Therefore, the present results suggest that the presence of the Br atom in position 5 favors the breaking of the ring, whereas the presence in position 2 favors the release of the halogen radical in a more efficient way for 2Br-pyrimidine compared with 2Cl-pyrimidine. The comparison between theoretical and experimental results makes it possible to suggest the correct fragmentation pathway to each measured cation fragment proposing the release of the $Br^{\bullet}$ radical in the brominated cases and of the $H^{\bullet}$ radical in the chlorinated case. These observations have also been rationalized in terms of (1) the interplay between the resonance and inductive effects induced on the pyrimidinic ring by the presence of the different halogen atom/site of halogenations; (2) the electronegativity of the halogen atoms.

The energetic properties are excellent indicators for fragmentation processes; nevertheless, a further study of molecular dynamics could be useful to achieve a complete view of the fragmentation patterns of these target molecules.

The present findings suggest that the choice of the most suitable radiosensitizer should be dictated by the goal of the therapy. In the case where interest is focussed on the environment surrounding the cell nucleus, the choice of the halogen in position 2 can lead to the release of the small H· radical or the more reactive Br· radical. On the other hand, if the purpose is the direct damage of the DNA chain, the 5Br-pyrimidine, which induces more significant breaking of the ring, is the most powerful choice.

## Acknowledgments

This work was partially supported by the MIUR PRIN 2009W2W4YF and 2009SLKFEX, MIUR FIRB RBFR10SQZI and European COST action MP1002 Nano-IBCT. The authors thank Dr. A. DeStefani for useful discussions and Mr. S. Rinaldi, R. Di Nino, and M. Petrucci for the prompt and qualified technical assistance.

## References

1. Bolognesi, P., O'Keeffe, P., Avaldi, L.: Soft X-ray Interaction with Organic Molecules of Biological Interest. In: Gomez-Tejedor, G.G., Fuss M.C. Eds. Radiation Damage in Biomolecular Systems, pp. 165. Springer Science + Business Media B.V, (2012)

2. Bodaïffa, B., Cloutier, P., Hunting, D., Huels, M.A., Sanche, L.: Resonant formation of DNA strand breaks by low-energy (3 to 20 eV) electrons. Science **287**, 1658–1660 (2000)
3. Hall, E.J., Giaccia, A.J.: Radiobiology for the Radiologist. Lippincott Williams Wilkins, pp. 35 (2005)
4. Serrano-Andrés, L., Merchán, M.: Are the five natural DNA/RNA base monomers a good choice from natural selection? A photochemical perspective. J. Photochem. Photobiol. C Photochem. Rev. **10**, 21–32 (2009)
5. Hudock, H.R., Levine, B.G., Thompson, A.L., Satzger, H., Townsend, D., Gador, N., Ullrich, S., Stolow, A., Martínez, T.J.: Ab initio molecular dynamics and time-resolved photoelectron spectroscopy of electronically excited uracil and thymine. J. Phys. Chem. **111**, 8500–8508 (2007)
6. Sanche, L.: Low energy electron-driven damage in biomolecules. Eur. Phys. J. D **35**, 367–390 (2005)
7. Abdoul-Carime, H., Huels, M.A., Illenberger, E., Sanche, L.: Sensitizing DNA to secondary electron damage: resonant formation of oxidative radicals from 5-halouracils. J. Am. Chem. Soc. **123**, 5354–5355 (2001)
8. Radisic, D., Jae Ko, Y., Nilles, J.M., Stokes, S.T., Sevilla, M.D., Rak, J., Bowen, K.H.: Photoelectron spectroscopic studies of 5-halouracil anions. J. Chem. Phys. **134**, 015101-1–015101-3 (2011)
9. Abdoul-Carime, H., Dugal, P.C., Sanche, L.: Damage induced by 1–30 eV electrons on thymine- and bromouracil-substituted oligonucleotides. Radiat. Res. **153**, 23–28 (2000)
10. O'Donoghue, J.A., Wheldon, T.E.: Targeted radiotherapy using Auger electron emitters. Phys. Med. Biol. **41**, 1973–1991 (1996)
11. Buchegger, F., Perillo-Adamer, F., Dupertuis, Y.M., Delaloye, A.B.: Auger radiation targeted into DNA: a therapy perspective. Eur. J. Nucl. Med. Mol. Imaging **33**, 1352–1363 (2006)
12. Bolognesi, P., O'Keeffe, P., Feyer, V., Plekan, O., Prince, K., Coreno, M., Mattioli, G., Amore Bonapasta, A., Zhang, W., Carravetta, V., Ovcharenko, Y., Avaldi, L.: Inner shell excitation, ionization and fragmentation of pyrimidine. J. Phys. Conf. Ser. **212**, 012002-1–012002-6 (2010)
13. Schwell, M., Joachims, H.-W., Baumagärtel, H., Leach, S.: VUV photophysics and dissociative photoionization of pyrimidine, purine, imidazole, and benzimidazole in the 7–18 eV photon energy range. Chem. Phys. **353**, 145–162 (2008)
14. Vall-llosera, G., Coreno, M., Erman, P., Huels, M.A., Jakubowska, K., Kivimäki, A., Rachlew, E., Stankiewicz, M.: VUV photoionization of free azabenzenes: pyridine, pyrazine, pyrimidine, pyridazine, and s-triazine. Int. J. Mass Spectrom. **275**, 55–63 (2008)
15. Linert, I., Dampc, M., Mielewska, B., Zubek, M.: Cross-sections for ionization and ionic fragmentation of pyrimidine molecules by electron collisions. Eur. Phys. J. D **66**, 20-1–20-9 (2012)
16. O'Keeffe, P., Bolognesi, P., Casavola, A.R., Catone, D., Zema, N., Turchini, S., Avaldi, L.: An experimental and computational study of the valence photoelectron spectra of halogenated pyrimidines. Mol. Phys. **107**, 2025–2037 (2009)
17. Stener, M., Decleva, P., Holland, D.M.P., Shaw, D.A.: A study of the valence shell electronic states of pyrimidine and pyrazine by photoabsorption spectroscopy and time-dependent density functional theory calculations. J. Phys. B Atomic Mol. Opt. Phys. **44**, 075203-1–075203-18 (2011)
18. Potts, A.W., Holland, D.M.P., Trofimov, A.B., Schirmer, J., Karlsson, L., Siegbahn, K.: An experimental and theoretical study of the valence shell photoelectron spectra of purine and pyrimidine molecules. J. Phys. B Atomic Mol. Opt. Phys. **36**, 3129–3146 (2003)
19. Bolognesi, P., O'Keeffe, P., Ovcharenko, E., Coreno, M., Avaldi, L., Feyer, V., Plekan, O., Prince, K.C., Zhang, W., Carravetta, V.: Pyrimidine and halogenated pyrimidines near edge X-ray absorption fine structure spectra at C and N K-edges: experiment and theory. J. Chem. Phys. **133**, 034302-1–034302-10 (2010)
20. Bolognesi, P., Mattioli, G., O'Keeffe, P., Feyer, V., Plekan, O., Ovcharenko, Y., Prince, K.C., Coreno, M., Amore Bonapasta, A., Avaldi, L.: Investigation of halogenated pyrimidines by X-ray photoemission spectroscopy and theoretical DFT methods. J. Phys. Chem. A **113**, 13593–13600 (2009)
21. Vall-llosera, G., Gao, B., Kivimäki, A., Coreno, M., Alvarez Ruiz, J., De Simone, M., Ågren, H., Rachel, E.: The C 1s and N 1s near edge X-ray absorption fine structure spectra of five azabenzenes in the gas phase. J. Chem. Phys. **128**, 044316-1–044316-12 (2008)
22. Storchi, L., Tarantelli, F., Veronesi, S., Bolognesi, P., Fainelli, E., Avaldi, L.: The Auger spectroscopy of pyrimidine and halogen-substituted pyrimidines. J. Chem. Phys. **129**, 154309-1–154309-10 (2008)
23. Tanaka, K., Sako, E.O., Ikenaga, E., Isari, K., Sardar, S.A., Wada, S., Sekitani, T., Mase, K., Ueno, N.: Control of chemical reactions by core excitations. J. Electron Spectrosc. Relat. Phenom. **119**, 255–266 (2001)
24. Tanaka, K., Kizaki, H., Sumii, R., Matsumoto, Y., Wada, S.: Atomic position dependence of the primary core electron excitation on site-specific chemical bond scission. Radiat. Phys. Chem. **75**, 2076–2079 (2006)
25. Nagaoka, S., Fukuzawa, H., Prumper, G., Takemoto, M., Takahashi, O., Yamaguchi, K., Kakiuchi, T., Tabayashi, K., Suzuki, I.H., Harries, J.R., Tamenori, Y., Ueda, K.: A study to control chemical reactions using Si:2p core ionization: site-specific fragmentation. J. Phys. Chem. A **115**, 8822–8831 (2011)
26. Plekan, O., Coreno, M., Feyer, V., Moise, A., Richter, R., de Simone, M., Sankari, E., Prince, K.: Electronic state resolved PEPICO spectroscopy of pyrimidine. Phys. Scr. **78**, 058105-1–058105-6 (2008)
27. Derossi, A., Lama, F., Piacentini, M., Prosperi, T., Zema, N.: High flux and high resolution beamline for elliptically polarized radiation in the vacuum ultraviolet and soft X-ray regions. Rev. Sci. Instrum. **66**, 1718–1720 (1995)
28. Available at: http://www.chemspider.com/ Accessed 13 Dec 2013
29. Marr, G.V., West, J.B.: Absolute photoionization cross-section tables for helium, neon argon, and krypton in the VUV spectral regions. At. Data Nucl. Data Tables **18**, 497–508 (1976)
30. Traeger, J.C., McLoughlin, R.G.: Absolute heats of formation for gas-phase cations. J. Am. Chem. Soc. **103**, 3647–3652 (1981)
31. Leach, S., Joachims, H., Baumgartel, H.: Photoionization mass spectrometric study of the prebiotic species formamide in the 10–20 eV Photon Energy Range. J. Phys. Chem. A **114**, 4847–4856 (2010)
32. Frisch, M.J., Trucks, G.W., Schlegel, H.B., Scuseria, G.E., Robb, M.A., Cheeseman, J.R., Scalmani, G., Barone, V., Mennucci, B., Petersson, G.A., Nakatsuji, H., Caricato, M., Li, X., Hratchian, H.P., Izmaylov, A.F., Bloino, J., Zheng, G., Sonnenberg, J.L., Hada, M., Ehara, M., Toyota, K., Fukuda, R., Hasegawa, J., Ishida, M., Nakajima, T., Honda, Y., Kitao, O., Nakai, H., Vreven, T., Montgomery, Jr., J. A., Peralta, J.E., Ogliaro, F., Bearpark, M., Heyd, J. J., Brothers, E., Kudin, K.N., Staroverov, V.N., Kobayashi, R., Normand, J., Raghavachari, K., Rendell, A., Burant, J. C., Iyengar, S. S., Tomasi, J., Cossi, M., Rega, N., Millam, J. M., Klene, M., Knox, J.E., Cross, J.B., Bakken, V., Adamo, C., Jaramillo, J., Gomperts, R., Stratmann, R. E., Yazyev, O., Austin, A. J., Cammi, R., Pomelli, C., Ochterski, J. W., Martin, R. L., Morokuma, K., Zakrzewski, V.G., Voth, G.A., Salvador, P., Dannenberg, J.J., Dapprich, S., Daniels, A.D., Farkas, O., Foresman, J.B., Ortiz, J.V., Cioslowski, J., Fox, D.J.: Revision A.1, Gaussian 09, Gaussian, Inc., Wallingford CT (2009)
33. Chupka, W.A.: Effect of thermal energy on ionization efficiency curves of fragment ions. J. Chem. Phys. **54**, 1936–1947 (1971)
34. Lias, S.G., Ausloos, P.: Ionization energies of organic compounds by equilibrium measurements. J. Am. Chem. Soc. **100**, 6027–6034 (1978)
35. Baboul, A.G., Curtiss, L.A., Redfem, P.C., Raghavachari, K.: Gaussian-3 theory using density functional geometries and zero-point energies. J. Chem. Phys. **110**, 7650–7657 (1999)
36. Bond, D.: Computational methods in organic thermochemistry. 1. Hydrocarbon enthalpies and free energies of formation. J. Org. Chem. **72**, 5555–5566 (2007)
37. Peng, C., Ayala, P.Y., Schlegel, H.B., Frisch, M.J.: Using redundant internal cordinates to optimize equilibrium geometries and transition states. J. Comp. Chem. **17**, 49–56 (1996)
38. Peng, C., Schlegel, H.B.: Combining synchronous transit and quasi-newton methods to find transition states. Israel J. Chem. **33**, 449–454 (1993)
39. Milani-Nejad, F., Stidham, H.D.: Spectra of $C_{2v}$, deuterium substituted pyrimidines. Spectrochim. Acta **31A**, 1433–1453 (1975)
40. Plekan, O., Feyer, V., Richter, R., Coreno, M., de Simone, M., Prince, K.C.: Photofragmentation of guanine, cytosine, leucine, and methionine. Chem. Phys. **334**, 53–63 (2007)